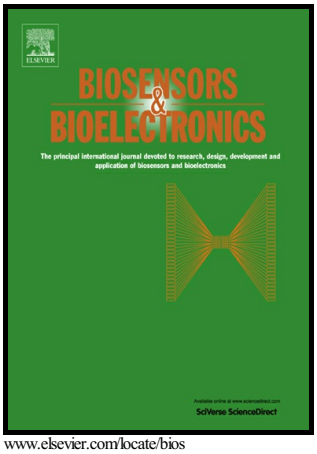

www.elsevier.com/locate/bios

A Novel Biosensor Based on Boronic Acid Functionalized Metal-Organic Frameworks for the Determination of Hydrogen Peroxide Released from Living Cells

Hongxia Dai, Wenjuan Lü, Xianwei Zuo, Qian Zhu, Congjie Pan, Xiaoying Niu, Juanjuan Liu, HongLi Chen, Xingguo Chen

PII: S0956-5663(17)30269-5
DOI: http://dx.doi.org/10.1016/j.bios.2017.04.021
Reference: BIOS9682

To appear in: *Biosensors and Bioelectronic*

Received date: 12 January 2017
Revised date: 23 March 2017
Accepted date: 17 April 2017

Cite this article as: Hongxia Dai, Wenjuan Lü, Xianwei Zuo, Qian Zhu, Congji Pan, Xiaoying Niu, Juanjuan Liu, HongLi Chen and Xingguo Chen, A Nove Biosensor Based on Boronic Acid Functionalized Metal-Organic Frameworks fo the Determination of Hydrogen Peroxide Released from Living Cells, *Biosensor and Bioelectronic,* http://dx.doi.org/10.1016/j.bios.2017.04.021

A Novel Biosensor Based on Boronic Acid Functionalized Metal-Organic Frameworks for the Determination of Hydrogen Peroxide Released from Living Cells

Hongxia Dai,[†,‡,II] Wenjuan Lü,[†,‡*] Xianwei Zuo,[†,‡] Qian Zhu,[†,‡] Congjie Pan,[†,‡] Xiaoying Niu,[†,‡] Juanjuan Liu,[†,‡] HongLi Chen,[†,‡] and Xingguo Chen[†,‡,§ *]

[†] State Key Laboratory of Applied Organic Chemistry, Lanzhou University, Lanzhou 730000, China

[‡] Department of Chemistry, Lanzhou University, Lanzhou 730000, China

[§] Key Laboratory of Nonferrous Metal Chemistry and Resources Utilization of Gansu Province, Lanzhou 730000, China

[II] Gansu University of Chinese Medicine, Lanzhou 730000, China

* Corresponding authors.

E-mail: chenxg@lzu.edu.cn (X. Chen), lvwenj@lzu.edu.cn (W. Lü).

Tel: 86-931-8912763

Fax: 86-931-8912582

Abstract: In this work, we report a durable and sensitive H_2O_2 biosensor based on boronic acid functionalized metal-organic frameworks (denoted as MIL-100(Cr)-B) as an efficient immobilization matrix of horseradish peroxidase (HRP). MIL-100(Cr)-B features a hierarchical porous structure, extremely high surface area, and sufficient recognition sites, which can significantly increase HRP loading and prevent them from

leakage and deactivation. The H_2O_2 biosensor can be easily achieved without any complex processing. Meanwhile, the immobilized HRP exhibited enhanced stability and remarkable catalytic activity towards H_2O_2 reduction. Under optimal conditions, the biosensor showed a fast response time (less than 4s) to H_2O_2 in a wide linear range of 0.5-3000 μM with a low detection limit of 0.1 μM, as well as good anti-interference ability and long-term storage stability. These excellent performances substantially enable the proposed biosensor to be used for the real-time detection of H_2O_2 released from living cells with satisfactory results, thus showing the potential application in the study of H_2O_2-involved dynamic pathological and physiological process.

***Keywords*:** Metal-organic frameworks, Boronic acid, Hydrogen peroxide, Horseradish peroxidase, Electrochemical biosensor.

1. Introduction

Hydrogen peroxide, as the most important representative of reactive oxygen species (ROS), can exert diverse pathological and/or physiological effects in living systems and participate in the physiological processes in a concentration-dependent manner (Giorgio et al., 2007; López-Lázaro 2007). Moderate levels of H_2O_2 are needed for intracellular signaling transduction and normal cell functions to maintain its integrity and survival (Reth 2002). However, excessive amounts of H_2O_2 can result

in oxidative stress, start toxic and lethal chain reactions, which is associated with the initiation and progression of many diseases, including neurodegenerative disorders, diabetes, atherosclerosis and cancers (Finkel 2000; Pagliari et al., 2012; Wu et al., 2010). Therefore, a rapid and accurate determination of H_2O_2 is of practical importance for a better understanding of the biological effect in cellular physiology and can further provide reliable diagnosis of pathological conditions.

In the past decades, various analytical techniques have been established for H_2O_2 sensing, such as chemiluminescence (Tsaplev 2012), fluorescence (Liang et al. 2016), colorimetry (Ge et al., 2015), surface-enhanced raman spectroscopy (Qu et al., 2016) and electrochemical techniques (Bai et al., 2016; Ju et al., 2015; Zhang et al., 2014). Among these methods, the electrochemical techniques are mostly used because of their high specificity, fast response, simplicity, convenient operation and on-spot analysis. In particular, an amperometric biosensor based on the redox proteins or enzymes (e.g., hemoglobin, horseradish peroxidase or cytochrome c) is an attractive tool for the detection of H_2O_2 due to their remarkable specificity and high sensitivity (Zhu et al., 2014). The immobilization of enzyme is very important for the preparation of enzyme-based biosensors. Compared to the free enzyme, immobilized enzyme shows better adaptability to the environment, the higher catalytic activity, and good repeated utilization.

Up to now, various types of materials, such as hydrogel (Jang et al., 2012), nanomaterials (Wang et al., 2003), clay minerals (Li et al., 2011), redox conducting polymers (Mazeiko et al., 2013) and even some kinds of porous materials (e.g., silica, molecular sieve or zeolites) (Benlarbi et al., 2012) have been investigated as immobilization supports for enzyme via different strategies. Nevertheless, to some extent, the problems of enzymatic loss, enzymatic inactivation, low stability as well as low mass-transfer efficiency of analytes are still involved within the reaction process (Chen et al., 2012; Yang et al., 2015). Therefore, the development of robust, stable, and efficient biocatalytic support platform has become a major research avenue to fabricate the enzyme biosensor.

Metal-organic frameworks (MOFs), consisting of inorganic nodes and organic ligands, have emerged as a class of porous materials with a wide application in gas storage and separation, catalysis (Furukawa et al., 2013). In comparison to other inorganic materials, this class of porous materials exhibits a high specific surface, ultrahigh porosity, structural tenability as well as diverse functionality via the activation or post-synthetic modification of the pendant groups of the organic linker. In virtue of these characteristics, MOFs have been one of the most promising immobilization matrix candidate for the fabrication of biosensors (Hou et al., 2015; Shen et al., 2015; Shieh et al., 2015; Wu et al., 2015; Xu et al., 2016). Unfortunately, most of MOFs are microporous

(pore diameter <2 nm), and the small size of their cavities restricts the choice of incorporated enzyme and induces low diffusion rates. In view of this, the mesoporous MOFs with sufficiently chemical/thermal stability (e.g., MIL-100 or MIL-101) are preferred, but leaching of the immobilized enzyme during the reaction process is still inevitable due to the absence of any specific interaction between enzyme and the support. This problem can be well solved through the functionalized modifications of a given MOFs, which provide functional group to aid to the desired adherence of enzymes. For example, the protease enzyme was successfully immobilized onto amino-functionalized MIL-88B(Cr) with 69% more catalytic efficiency than free form over four cycles (Shih et al., 2012). Recently, the developed metal-ligand-fragment co-assembly (MLFC) strategy could effectively work to introduce a wide variety of functional groups into MOFs, in which the primitive ligand and its ligand fragment were co-assembled to generate a series of the isostructural MOFs (Fang et al., 2014; Park et al., 2012). This strategy has been successfully used to introduce accessible boronic acid functionality into MIL-100(Cr) for the purification, sensing and separation of sugars (Zhu et al., 2015). Hence, the combination of the porous MOFs and the recognition of boric acid to cis-diol could be served as an effective mean to immobilize glycoprotein and applied to improve the analytical performance of the biosensor. However, to our best knowledge, there is

still no relevant report in this respect.

Herein, boronic acid functionalized MOFs, a sponge-like MIL-100(Cr)-B, was firstly used as a novel immobilization matrix of horseradish peroxidase (HRP) to fabricate a H_2O_2 biosensor. UV-vis and electrochemical measurements showed that the incorporation of boronic acid moieties can significantly increase the amount of HRP loading and improve the stability of the biosensor. Most importantly, the immobilized HRP had high bio-catalytic activity toward the reduction of H_2O_2, leading to a fast, selective and sensitive amperometric response to H_2O_2 with a wide linear range. By virtue of these merits, this H_2O_2 biosensor has been successfully applied in the real-time detection of H_2O_2 released from living cells.

2. Experimental

2.1 Materials

5-Boronobenzene-1,3-dicarboxylic acid (BBDC) was purchased from Energy Chemical Reagents Company (Shanghai, China). 1,3,5-benzene tricarboxylic acid (BTC), chrormic trioxide (CrO_3), HF (40%), HRP (E.C. 1.11.1.7, Type VI, 300 U mg^{-1}), 3-(4,5-dimethyl-2-thiazolyl)-2,5-diphenyl-2H-tetrazolium bromide (MTT) and catalase (E.C. 1.11.1.6, from bovine liver, 3000 U mg^{-1}) were purchased from Sigma (St. Louis, MO, USA). Phorbol 12-myristate

13-acetate (PMA) was purchased from Wako Pure Chemical Industries (Osaka, Japan). RAW 264.7 murine macrophages, human cervical cancer cells (Hela) and human breast cancer cells (MCF-7) were obtained from Gansu University of Chinese Medicine (Lanzhou, China). Amplex Red Hydrogen Peroxide Assay kit was purchased from Thermo Fisher (Shanghai, China). All other reagents were of analytical grade and used without further purification. All solutions were prepared with ultra-pure water (18 MΩ, Milli-Q purification system, Bedford, MA, USA).

2.2 Apparatus

The morphologies and surface structures were characterized with field-emission scanning electron microscope (SEM, ZEISS, Germany). Powder X-ray diffraction (PXRD) analysis was performed on a Bruker D8 Advance Diffractometer (Germany). X-ray photoelectron spectroscopy analysis (XPS) was carried out with ESCALAB Mark II (VG Scientific, UK). The N_2 sorption-desorption isotherms was performed on an ASAP 2020 instrument (Micromeritics, USA). The Brunauer-Emmett-Teller (BET) method was used to calculate the specific surface area. The FT-IR spectra were collected on a Nicolet-670 Fourier transform FT-IR spectrophotometer in KBr disks (Thermo, USA). UV-vis measurements were carried out on UV-1700 PharmaSpec spectrophotometer (Shimadzu Co., Ltd, Japan). Thermogravimetric

analysis (TGA) was taken with a thermogravimetric analyzer (Perkin-Elmer TGA-7, USA). Zeta-potential measurements were conducted using a Zetasizer Nano ZS analyzer (Malvern Inst., UK).

All electrochemical measurements were performed with CHI 660D electrochemical workstation (Chenhua Instruments Co., Shanghai, China) at room temperature. A conventional three-electrode cell was used with modified glass carbon electrode (GCE, 3 mm diameter) as the working electrode, saturated calomel electrode (SCE) as the reference electrode, and platinum wire as the counter electrode. A 0.1 M phosphate buffer solution (PBS, pH 7.4) comprising NaH_2PO_4 and Na_2HPO_4 was used as the supporting electrolyte and the electrolyte was bubbled with highly purity nitrogen for at least 20 min prior to use. Cyclic voltammetry (CV) was carried out in 0.1 M PBS with or without 0.1 mM H_2O_2 from 0.2 to -0.8 V at scanning rate of 100 mV s^{-1}. Electrochemical impedance spectroscopy (EIS) was carried out in 5 mM $K_3Fe(CN)_6/K_4Fe(CN)_6$ containing 0.1 M KCl at 0.20 V (*vs.* SCE) with a frequency range of 0.1-100 kHz. All amperometric measurements were regularly carried out at -0.30 V on a stirred cell. After reaching steady-state current, the aliquots of H_2O_2 standard solution were successively added to the solution, and the change in the current signal was monitored.

2.3 Synthesis of MIL-100(Cr)-B

MIL-100(Cr)-B was prepared by a modified method based on previous reports (Vimont et al., 2006; Zhu et al., 2015). Briefly, 100.0 mg CrO_3, 56.3 mg BBDC, 101.4 mg BTC and 4.8 mL H_2O were introduced into a 25 mL Teflon reactor. After stirring for 2 h, 22 μL HF solution (40%) was added to the mixture. The reactor was sealed and heated in an oven at 200 °C for 72 h. After cooled down to room temperature, the obtained green solid was collected by centrifugation, thoroughly washed with dimethyl formamide, hot water and acetone several times. Then, the obtained green solid was dried under vacuum overnight. The native MIL-100(Cr) was prepared with 169.0 mg BTC by the same procedure in the above description, while no BBDC was added in the starting synthesis system.

2.4 Evaluation of MOFs on enzyme loading capacity

One milligram of native MIL-100(Cr) or MIL-100(Cr)-B was separately dispersed into 1.0 mL of aqueous solution of HRP (2.0 mg mL^{-1}). The resulting mixtures were agitated at room temperature for 30 min. The supernatants were collected and diluted for 25 times for UV-Vis spectroscopic measurements. The amount of enzyme loading was evaluated indirectly by the decrease values of the absorbance at 403 nm.

2.5 Fabrication of enzyme electrode

The fabrication of the enzyme electrode was performed by a simple and low-cost approach. Firstly, 10 μL HRP solution (2.0 mg mL^{-1}) was added into 10 μL MIL-100(Cr)-B suspension (1.0 mg mL^{-1}), and the mixture was shaken for 30 min. Secondly, 8 μL of the mixture was drop-coated on the GC electrode surface and dried at room temperature. Subsequently, 2 μL of 0.05% Nafion solution was dropped onto the modified electrode surface to form a protective layer. After being dried in air, the electrode was rinsed three times with ultrapure water to remove the loosely absorbed HRP. The obtained HRP-MIL-100(Cr)-B/GCE was stored at 4 °C in a refrigerator for use. For comparison, HRP/GCE, MIL-100(Cr)/GCE, MIL-100(Cr)-B/GCE, and HRP-MIL-100(Cr)/GCE were prepared in the similar way.

2.6 Detection of H_2O_2 released from living Cells

RAW 264.7 murine macrophage, Hela and MCF-7 cells were cultured in Dulbecco's modified Eagle medium containing 10% (v/v) fetal bovine serum, 100 U mL^{-1} penicillin, and 100 mg mL^{-1} streptomycin at 37 °C in a 5% CO_2 environment.

After growing to 90% confluence, the cells were collected by centrifugation and washed three times with PBS (10 mM, pH 7.4). Cell number was estimated by a hemocytometer. During the test, a pellet that each contained *ca.* 1×10^6 cells was resuspended into 10.0 mL of PBS (0.1

M, pH 7.4) and the mixture was deoxygenated by gently shaking the cells under a humidified nitrogen stream. A potential of -0.30 V (*vs.* SCE) was applied to the HRP-MIL-100(Cr)-B/GCE. After a steady-state current achieved, PMA was injected into the cells suspension to stimulate cells to produce H_2O_2 and the change in the current signal was monitored as shown in Scheme 1. As a control group, 50 μL of catalase (300 U mL^{-1}) was then added to the solution that contained cells.

(Please insert **Scheme 1** here)

3. Results and discussion

3.1 Characterization of HRP-MIL-100(Cr)-B

The synthesized MIL-100(Cr) and MIL-100(Cr)-B were characterized by XRD, XPS, SEM, TGA and N_2 adsorption-desorption isotherm (Figs. S1-S3). It can be seen that both MIL-100(Cr) and MIL-100(Cr)-B have larger specific surface area (>1400 m^2 g^{-1}) and hierarchically porous structures, which are beneficial of the adsorption of HRP. In Fig. 1A, the enzyme loading ability of the two materials was evaluated by UV-Vis spectra. HRP showed the characteristic Soret band at 403 nm (curve a). After the addition of the same amount of MIL-100(Cr) or MIL-100(Cr)-B, the absorbance of this peak for its supernatants decreased, suggesting that porous MOFs could serve as

support matrix for HRP (curve b and c). The amount of HRP incorporated in MIL-100(Cr)-B film was calculated to be 1.78 mg mg^{-1} (HRP wt. /MOFs wt.), which was larger than that in MIL-100(Cr) (1.12 mg mg^{-1}) according to Lambert-Beer's law (Fig. S4). The enhanced loading ability of MIL-100(Cr)-B towards HRP, substantially demonstrated the necessity of integrating boronic acid moiety within MIL-100(Cr) framework. Besides, it has been reported that HRP is positively charged at neutral pH (Song et al., 2006). In contrast, MIL-100(Cr)-B possessed a negative charge of -21.0 mV at this pH and the zeta potential gradually reduced to -10.4 mV with the increase of the amount of HRP adsorbed on MIL-100(Cr)-B (Fig. S5). The zeta potential measurements revealed that the electrostatic interaction existed between HRP and MIL-100(Cr)-B. After immobilization, another important consideration was the enzyme should retain its secondary structure. From the FT-IR spectroscopy in Fig. 1B (curve a), isostructural MIL-100(Cr)-B presented the characteristic bands of carboxylate coordination at 3400, 1390, and 1449 cm^{-1}, and Cr-O bonds at ~523 and ~563 cm^{-1}. However, the typical vibrational band of B-O (1350-1310 cm^{-1}) was inconspicuous, which could be ascribed to the partial overlap by the strong stretching vibration (C=O) of trimesate ligand. For pure HRP, the amide I band (1700-1600 cm^{-1}) is assigned to a protein with α-helical conformation, whereas the amide II band (1620-1500 cm^{-1}) is due to the parallel β-sheet structure of HRP (curve b)

(Adams et al., 2002). As expected, the major bands of HRP were observed in the spectra of HRP-MIL-100(Cr)-B composite (curve c), suggesting that HRP was successfully immobilized on the MIL-100(Cr)-B without denaturation of its secondary structure or the basic backbone structure of MIL-100(Cr)-B. When a portion of the free space in MIL-100(Cr)-B was occupied by HRP molecules, the BET surface area decreased from 1413 m^2 g^{-1} to 1007 m^2 g^{-1} (Table S1). Meanwhile, the bigger mesopores of MIL-100(Cr)-B partially disappeared whereas most micropores remained predominantly around 0.72 nm (Fig. 1C). This micropore structure was conductive to accelerate the diffusion rate of substrates to access the active centers of HRP. The SEM image clearly displayed the HRP-MIL-100(Cr)-B composite has a similar spongy porous structure with some obvious agglomerates, corresponding to the assembly of HRP on the surface of MIL-100(Cr)-B (Fig. 1D). The electrochemical impedance spectroscopy (EIS) technique was performed to explore the interface properties of surface modified electrodes. As shown in Fig. S6, the rather insulating nature of immobilized HRP greatly hindered the electron transfer of the redox probe to the electrode surface, resulting in significant increase of the charge transfer resistance (R_{ct}) of $Fe(CN)_6^{3-/4-}$ redox couple. The results fully demonstrated the proposed biosensor was constructed as expected, and the following studies showed that the enzyme retained its high

activity after immobilization.

(Please insert **Fig. 1** here)

3.2 Bioelectrocatalytic activity of HRP-MIL-100(Cr)-B/GCE towards H_2O_2

The CV responses of different electrodes have been investigated in 0.1 M PBS (pH 7.4) from 0.2 to -0.8 V at scan rate of 100 mV s^{-1}. No redox peaks were observed at MIL-100(Cr)/GCE or MIL-100(Cr)-B/GCE, indicating that both MIL-100(Cr) and MIL-100(Cr)-B were electrochemically inactive (Fig. 2A). On the other hand, all of the enzyme electrodes showed an obvious cathodic peak at *ca.* -0.35 V corresponding to the reduction of HRP. Especially for HRP-MIL-100(Cr)-B/GCE, the reduction peak current was much larger than those of the HRP/GCE and HRP-MIL-100(Cr)/GCE. Meanwhile, the reversibility of the electrochemical reaction was enhanced and accompanied with a small oxidation peak at -0.188 V. These results elucidated that the porous MIL-100(Cr)-B film could provide a biocompatible microenvironment and accelerate the electron transfer between the heme in HRP and the electrode. However, a well-defined and symmetric shape of CVs has not yet been obtained at HRP-MIL-100(Cr)-B/GCE. This phenomenon may be ascribed to a small amount of residual oxygen presented within the MOFs, which cannot achieve a complete release even heating at 323 K

under dynamic vacuum (Murray et al. 2011). The electrochemical stability of HRP, HRP-MIL-100(Cr) and HRP-MIL-100(Cr)-B based electrodes were shown in Fig. 2B. Only HRP-MIL-100(Cr)-B retained more than 90% of its initial peak current at -0.30 V during consecutive potential scanning up to 100 cycles at scan rate of 100 mV s^{-1}. Since it has been reported that HRP, a typical glycoprotein, can be specifically immobilized to different support through boronic acid-sugar interactions (Cui et al., 2011; Liu et al., 2006; Liu et al., 2005), it is reasonable to speculate that both the residual boronic acid group and the porous structure of MIL-100(Cr)-B are the essential cause for the better bioactivity and electrochemical stability.

In addition, we studied the effect of scan rate (v) on CV responses (Fig. 2C). The reduction peak currents exhibited a linear relationship with the scan rate in the range from 20 to 300 mV s^{-1}, suggesting that the electrochemical reaction of HRP entrapped in MIL-100(Cr)-B film was a typical surface-controlled process. Upon the addition of 0.1 mM H_2O_2, the catholic peak current increased significantly, corresponding to the electrocatalytic reduction of H_2O_2 (solid line in Fig. 2D). The response to H_2O_2 of HRP-MIL-100(Cr)-B/GCE was 2.5 times larger than that of HRP-MIL-100(Cr)/GCE, whereas the response at the MIL-100(Cr) or MIL-100(Cr)-B modified electrode were both extremely weak. These results suggested that HRP entrapped in the porous MIL-100(Cr)-B

nanostructure showed the higher catalytic activity.

(Please insert **Fig. 2** here)

Interestingly, the electrocatalytic reduction behavior for dissolved oxygen at HRP-MIL-100(Cr)-B/GCE was almost the same as that of H_2O_2 (Fig. S7). The reduction peak current increased with the amount of dissolved oxygen in the solution, indicating the similarity of reaction mechanism between the two systems. According to previous reports (Zhang et al., 2004; Yin et al., 2009; Nakajima et al., 1987; Huang et al., 2003), the possible mechanism of electrocatalytic reduction of H_2O_2 in this work can be expressed as follows:

$$HRP(Fe^{III}) + H_2O_2 \rightarrow \text{Compound } \mathbf{I}\ (Fe^{IV} = O, P^{\bullet+}) + H_2O \quad (1)$$

$$\text{Compound } \mathbf{I}\ (Fe^{IV} = O, P^{\bullet+}) + H_2O_2 \rightarrow HRP(Fe^{III}) + O_2 \quad (2)$$

$$HRP(Fe^{III}) + e^- + H^+ \rightarrow HRP(Fe^{II}) \quad \text{at electrode} \quad (3)$$

$$HRP(Fe^{II}) + O_2 \rightarrow HRP(Fe^{II}\text{-}O_2) \quad \text{fast} \quad (4)$$

$$HRP(Fe^{II}\text{-}O_2) + 2e^- + 2H^+ \rightarrow HRP(Fe^{II}) + H_2O_2 \quad \text{at electrode} \quad (5)$$

3.3 Amperometric biosening of H_2O_2

The amperometric method was used to evaluate the analytical performance of HRP-MIL-100(Cr)-B/GCE towards the detection of H_2O_2. The electrolyte was bubbled with highly purity nitrogen to removal the oxygen dissolved in the electrolyte prior to use. To obtain optimal

amperometric response to H_2O_2, the effect of immobilized amount of HRP, the solution pH and the applied potential on the response current of HRP-MIL-100(Cr)-B/GCE were investigated as shown in Fig. S7 (details in supporting information). Fig. 3A displayed the typical amperometric response at HRP-MIL-100(Cr)-B/GCE upon successive addition of H_2O_2 into the stirred 0.1 M PBS (pH 7.4) at the applied potential of -0.30 V. The proposed electrode yielded a step-like increase in current response and the time to reach 90% of the maximum current was within 4 s, indicative of a fast response process. The amperometric response was linear with H_2O_2 concentration from 0.5 μM to 3.0 mM with a correlation coefficient of 0.998 (Fig. 3B). The biosensor exhibited a high sensitivity of 47.9 μA mM^{-1} and the limit of detection was estimated to be 0.1±0.02 μM at a signal-to-noise ratio of 3.

The amperometric response attained saturation levels at higher concentrations, representing a typical Michaelis-Menten enzymatic reaction characteristic. For amperometric biosensors, algebraic Eadie-Hofstee transformation of the Michaelis-Menten equation can be expressed as follows (Mao et al., 2013): $1/I_{\mathrm{m}}=1/I_{\mathrm{max}}+K_{\mathrm{M}}^{\mathrm{app}}/(CI_{\mathrm{max}})$, where I_{m} is the steady-state current, C is the concentration of substrate, $K_{\mathrm{M}}^{\mathrm{app}}$ is the apparent Michaelis-Menten constant, and I_{max} is the intercept on the current axis. $K_{\mathrm{M}}^{\mathrm{app}}$ was calculated to be 0.46 mM for HRP entrapped in MIL-100(Cr)-B, The lower $K_{\mathrm{M}}^{\mathrm{app}}$ value further

confirmed that HRP immobilized on the MIL-100(Cr)-B nanostructures had high affinity to H_2O_2. Compared to other HRP-based biosensors (Table S2), the HRP-MIL-100(Cr)-B/GCE biosensor exhibited a wider linear range, lower limit of detection, applied potential and K_M^{app}. These excellent performances could be ascribed to the accelerated diffusion rate of substrate and well-retained bioactivity of the HRP immobilized in the biocompatible porous MIL-100(Cr)-B film. Moreover, the strong binding between MIL-100(Cr)-B and HRP minimized the leakage of HRP and improved the electron transfer between enzyme and electrode, which was also beneficial to the sensitivity of the developed biosensor.

(Please insert **Fig. 3** here)

To assess the possible analytical application of the developed H_2O_2 biosensor, the effects of the most commonly existing interferents in the physiological environment have been examined. Fig. S9 displayed the current response of 1.0 mM H_2O_2 and 0.5 mM of glucose (Glu), ascorbic acid (AA), dopamine (DA), uric acid (UA), L-Glutathione reduced (GSH) and $NaNO_2$ at the HRP-MIL-100(Cr)-B/GCE. No obvious current responses of these coexisting species were observed, highlighting the remarkable specificity of the biosensor toward H_2O_2. The superior selectivity could be attributed to the specificity of enzymes reactions and the negatively charged HRP-MIL-100(Cr)-B with microporous structure,

which acts as an effective pre-selective barrier to reduce interference from the anionic species and macromolecules in biological samples. The stability and reproducibility of the HRP-MIL-100(Cr)-B/GCE were also investigated by measuring the response to 0.1 mM H_2O_2. After storage at 4 °C for a month, 90% of the initial current response retained and the current response remained stable for almost 1000 s (Fig. S10), indicating the long-term storage stability of the biosensor. Besides, the reproducibility expressed in terms of relative standard deviation (RSD) of the same electrode in 10 successive measurements was 0.4%, while 3.4 % for 10 electrodes fabricated from different batches, respectively. This suggested that the proposed biosensor possessed good precision and acceptable reproducibility.

3.4 Measurements of H_2O_2 released from living cells

To explore the application of the HRP-MIL-100(Cr)-B biosensor, the detection of H_2O_2 in living cells was performed. Before that, MTT (3-(4,5-dimethylthiazol-2-yl)-2,5-diphenyltetrazolium bromide) assay was used to measure the cytotoxicity of HRP-MIL-100(Cr)-B. As displayed in Fig. S11, after culturing with HRP-MIL-100(Cr)-B (8 μL, 1.5 mg mL^{-1}) for 24 h, the living cells showed an excellent cell viability of >90%, indicative of the good biocompatibility of HRP-MIL-100(Cr)-B. Taking RAW 264.7 macrophage as an example, PMA was employed as a

stimulating agent, which can induce the H_2O_2 generation from living cells within a short period of time (Maji et al., 2014; Wu et al., 2012). When 50 μL 200 ng mL^{-1} PMA was injected into the PBS medium containing RAW 264.7 macrophage, a significant change of amperometric response was obtained (curve a in Fig. 4A). The maximum current of ~59 nA was obtained in 50 s, corresponding to ~1.2 μM (n=3) H_2O_2 released from the cells. Interestingly, if catalase solution (50 μL, 300 U mL^{-1}), a selective scavenger of H_2O_2, was premixed with the PBS that contained cells, no measurable change in current response was observed after the injection of PMA (curve b). This phenomenon further confirmed that the obvious current change was only due to the H_2O_2 production from the cells. Under the same conditions, the current responses were also measured for Hela and MCF-7 cells, and the comparison was shown in Fig. 4B. The current signal change from these two cancer cells were more notable than RAW 246.7 cells, indicating that that abnormal growth of the tumor has an enhancement of H_2O_2 production ability. This is meaningful for the development of cancer chemopreventive and therapeutic strategies. As a contrast, the released amounts of H_2O_2 were further evaluated by using the reference fluorescence method (Table 1). The relative deviations of the two methods are less than 4%, which showed the proposed biosensor was reliable in detecting H_2O_2 released from living cells, and has potential application in the study of H_2O_2-involved dynamic pathological

and physiological process.

(Please insert **Fig. 4** here)

(Please insert **Table 1** here)

4. Conclusions

In summary, we successfully prepared a robust H_2O_2 biosensor using MIL-100(Cr)-B as highly efficient immobilization matrix of HRP without addition of any mediator. The hierarchical porous structure of MIL-100(Cr)-B associated with sufficient active sites not only increased the amount of immobilized enzyme, but also provided a biocompatible microenvironment for HRP and a pathway for H_2O_2 diffusion. The developed HRP-MIL-100(Cr)-B/GCE exhibited excellent performance and good stability for quick and specific detection of H_2O_2. The fabricated biosensor has been successfully used for the monitoring the trace level of H_2O_2 released from living cells, which demonstrates the great potential of functionalized MOFs for fabricating reliable enzyme biosensors.

Acknowledgments

The authors are grateful for financial support from the National Natural Science Foundation of China (No. 21375053) and the Specialized

Research Fund for the Doctoral Program of Higher Education (No. 20130211110039).

References

Adams, S., Higgins, A. M., Jones, R. A. L., 2002. Langmuir 18, 4854-4861.

Bai, Z., Li, G., Liang, J., Su, J., Zhang, Y., Chen, H., Huang, Y., Sui, W., Zhao, Y., 2016. Biosens. Bioelectron. 82, 185-194.

Benlarbi, M., Blum, L. J., Marquette, C. A., 2012. Biosens. Bioelectron. 38, 220-225.

Cui, L., Xu, M., Zhu, J., Ai, S., 2011. Synthetic Metals 161, 1686-1690.

Fang, Z., Dürolt, J. P., Kauer, M., Zhang, W., Lochenie, C., Jee, B., Albada, B., Metzler-Nolte, N., Pöppl, A., Weber, B., 2014. J. Am. Chem. Soc. 136, 9627-9636.

Finkel, T., 2000. FEBS Lett. 476, 52-54.

Furukawa, H., Cordova, K. E., O'Keeffe, M., Yaghi, O. M., 2013. Science 341, 974-987.

Ge, S., Liu, W., Liu, H., Liu, F., Yu, J., Yan, M., Huang, J., 2015. Biosens. Bioelectron. 71, 456-462.

Giorgio, M., Trinei, M., Migliaccio, E., Pelicci, P. G., 2007. Nat. Rev. Mol. Cell Biol. 8, 722-728.

Horcajada, P., Serre, C., Vallet-Regí, M., Sebban, M., Taulelle, F., Férey, G., 2006. Angew. Chem. 118, 6120-6124.

Hou, C., Wang, Y., Ding, Q., Jiang, L., Li, M., Zhu, W., Pan, D., Zhu, H.,

Liu, M., 2015. Nanoscale 7, 18770-18779.

Huang, R., Hu, N., 2003. Biophys. Chem. 104, 199-208.

Jang, E., Kim, S., Koh, W.-G., 2012. Biosens. Bioelectron. 31, 529-536.

Ju, J., Chen, W., 2015. Anal. Chem. 87, 1903-1910.

López-Lázaro, M., 2007. Cancer Lett. 252, 1-8.

Li, C., Zhang, H., Wu, P., Gong, Z., Xu, G., Cai, C., 2011. Analyst 136, 1116-1123.

Liang, L., Lan, F., Li, L., Su, M., Ge, S., Yu, J., Liu, H., Yan, M., 2016. Biosens. Bioelectron. 82, 204-211.

Liu, S., Bakovic, L., Chen, A., 2006. J. Electroanal. Chem. 591, 210-216.

Liu, S., Miller, B., Chen, A., 2005. Electrochem. Commun. 7, 1232-1236.

Llewellyn, P. L., Bourrelly, S., Serre, C., Vimont, A., Daturi, M., Hamon, L., De Weireld, G., Chang, J. S., Hong, D. Y., Kyu Hwang, Y., 2008. Langmuir 24, 7245-7250.

Maji, S. K., Sreejith, S., Mandal, A. K., Ma, X., Zhao, Y. L., 2014. ACS Appl. Mater. Interfaces 6, 13648-13656.

Mao, S., Long, Y., Li, W., Tu, Y., Deng, A., 2013. Biosens. Bioelectron. 48, 258-262.

Mazeiko, V., Kausaite-Minkstimiene, A., Ramanaviciene, A., Balevicius, Z., Ramanavicius, A., 2013. Sens. Actuators B 189, 187-193.

Murray, L. J., Dinca, M., Yano, J., Chavan, S., Bordiga, S., Brown, C. M., Long, J. R., 2010. J. Am. Chem. Soc. 132, 7856-7857.

Nakajima, R., Yamazaki, I., J. Biol. Chem. 262, 2576-2581.

Pagliari, F., Mandoli, C., Forte, G., Magnani, E., Pagliari, S., Nardone, G., Licoccia, S., Park, J., Wang, Z. U., Sun, L. B., Chen, Y. P., Zhou, H. C., 2012. J. Am. Chem. Soc. 134, 20110-20116.

Park, J., Wang, Z. U., Sun, L. B., Chen, Y. P., Zhou, H. C., 2012. J. Am. Chem. Soc. 134, 20110-20116.

Qu, L. L., Liu, Y. Y., He, S. H., Chen, J. Q., Liang, Y., Li, H. T., 2016. Biosens. Bioelectron. 77, 292-298.

Reth, M., 2002. Nat. Immunol. 3, 1129-1134.

Shen, W. J., Zhuo, Y., Chai, Y. Q., Yuan, R., 2015. Anal. Chem. 87, 11345-11352.

Shieh, F. K., Wang, S. C., Yen, C. I., Wu, C. C., Dutta, S., Chou, L. Y., Morabito, J.V., Hu, P., Hsu, M. H., Wu, K. C. W., 2015. J. Am. Chem. Soc. 137, 4276-4279.

Shih, Y. H., Lo, S. H., Yang, N. S., Singco, B., Cheng, Y. J., Wu, C. Y., Chang, I., Huang, H. Y., Lin, C. H., 2012. ChemPlusChem 77, 982-986.

Song, Y. H., Wang, L., Ren, C. B., Zhu, G. Y., Li, Z., 2006. Sens. Actuators B 114, 1001-1006.

Tsaplev, Y.B., 2012. Anal. Chem. 67, 506-514.

Vimont, A., Goupil, J. M., Lavalley, J. C., Daturi, M., Surblé, S., Serre, C., Millange, F., Férey, G., Audebrand, N., 2006. J. Am. Chem. Soc. 128,

3218-3227.

Wang, J., Musameh, M., Lin, Y., 2003. J. Am. Chem. Soc. 125, 2408-2409.

Wang, Y., Ma, X., Wen, Y., Xing, Y., Zhang, Z., Yang, H., 2010. Biosens. Bioelectron. 25, 2442-2446.

Wu, P., Qian, Y., Du, P., Zhang, H., Cai, C., 2012. J. Mater. Chem. 22, 6402-6412.

Wu, X., Ge, J., Yang, C., Hou, M., Liu, Z., 2015. Chem. Commun. 51, 13408-13411.

Wu, X., Hu, Y., Jin, J., Zhou, N., Wu, P., Zhang, H., Cai, C., 2010. Anal. Chem. 82, 3588-3596.

Xu, R., Wang, Y., Duan, X., Lu, K., Micheroni, D., Hu, A., Lin, W., 2016. J. Am. Chem. Soc. 138, 2158-2161.

Yin, H., Ai, S., Shi, W., Zhu, L., 2009. Sens. Actuators B 137, 747-753.

Yang, C., Dennol, M. E., Pyakurel, P., Jill Venton, B., 2015. Anal. Chim. Acta 887, 17-37.

Zhang, Y., Bai, X., Wang, X., Shiu, K.-K., Zhu, Y., Jiang, H., 2014. Anal. Chem. 86, 9459-9465.

Zhang, Y., He, P. L., Hu, N. F., 2004. Electrochim. Acta 49, 1981-1988.

Zhu, C., Yang, G., Li, H., Du, D., Lin, Y., 2014. Anal. Chem. 87, 230-249.

Zhu, X., Gu, J., Zhu, J., Li, Y., Zhao, L., Shi, J., 2015. Adv. Funct. Mater. 25, 3847-3854.

Table 1. Determinaton of H_2O_2 released from living cells (1×10^6). (n=3)

Sample	Proposed biosensor (μM)	Fluorescence method* (μM)	Relative deviation (%)
RAW 264.7	1.20	1.24	-3.22
Hela cells	1.98	2.05	-3.41
MCF-7 cells	2.43	2.38	2.10

* Extracellular hydrogen peroxide levels were measured using an Amplex Red Hydrogen Peroxide Assay kit (Molecular Probes) according to the manufacturer's.

Figure Captions

Scheme 1. Schematic of the HRP-MIL-100(Cr)-B modified GCE used for detecting H_2O_2 release from cells stimulated with PMA. Chromium, carbon, oxygen and boron atoms are depicted as green, gray, red and blue spheres, respectively.

Fig. 1. (A) UV-Vis absorption spectra of original HRP solution (a) and its supernatants obtained with the addition of 1.0 mg of MIL-100(Cr) (b) or MIL-100(Cr)-B (c). (B) FT-IR spectra of MIL-100(Cr)-B (a), HRP (b) and HRP-MIL-100(Cr)-B (c). (C) Distribution of pore diameters and (D) SEM images of HRP-MIL-100(Cr)-B composite.

Fig. 2. (A) CVs of bare GCE, MIL-100(Cr), MIL-100(Cr)-B, HRP, HRP-MIL-100(Cr) and HRP-MIL-100(Cr)-B modified electrode in 0.1 M PBS (pH 7.4) at scan rate of 100 mV s^{-1}. (B) Consecutive CV response of HRP, HRP-MIL-100(Cr) and HRP-MIL-100(Cr)-B modified electrode in 0.1 M PBS (pH 7.4) at scan rate of 100 mV s^{-1} through 100 cycles. (C) CVs of HRP-MIL-100(Cr)-B/GCE in 0.10 M PBS buffer (pH 7.4) at the scan rates from 20 to 300 mV s^{-1}. Inset: I_{pc} versus ν. (D) CV response of HRP-MIL-100(Cr) (a, c) and HRP-MIL-100(Cr)-B (b, d) with (solid line) or without (dash-dotted line) addition of 0.1 mM H_2O_2 in 0.1 M PBS (pH 7.4) at scan rate of 100 mV s^{-1}.

Fig. 3. (A) Amperometric response of the HRP-MIL-100(Cr)-B/GCE with successive addition of different concentrations of H_2O_2 at the potential of -0.30 V. (Inset: a partial magnification of the current response toward a low concentration of H_2O_2 solution). (B) The corresponding calibration curve for H_2O_2 sensing. (Inset: Determination of

K_M^{app} for HRP).

Fig. 4. (A) Typical amperometric responses of the HRP-MIL-100(Cr)-B/GCE for the reduction of H_2O_2 release from Raw 264.7 cells induced by PMA without (a) and with (b) addition of catalase at -0.30 V (*vs.* SCE). (B) Comparing the catalytic current response of the H_2O_2 released from RAW 264.7 macrophage, Hela, and MCF-7 cells.

Scheme 1.

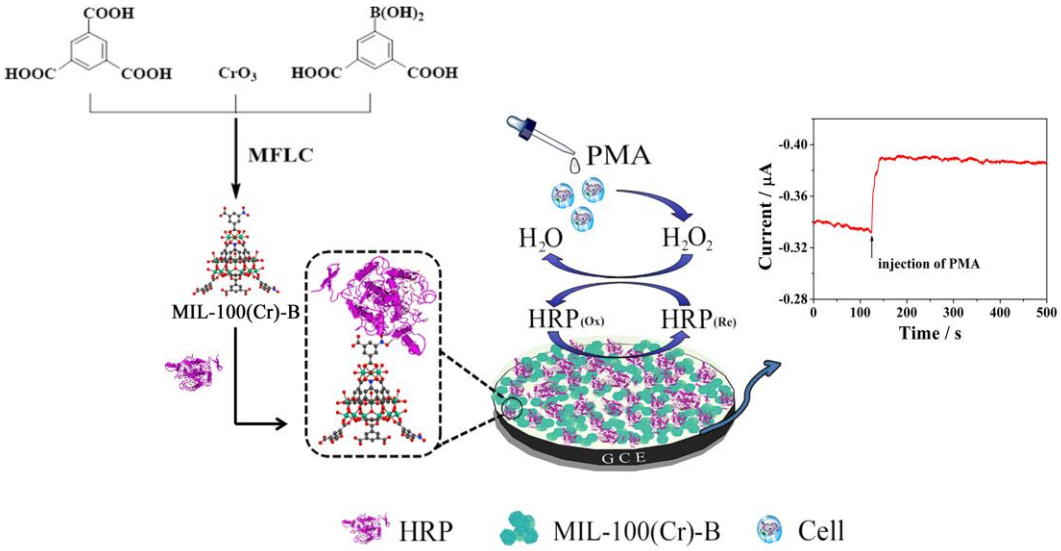

Fig. 1.

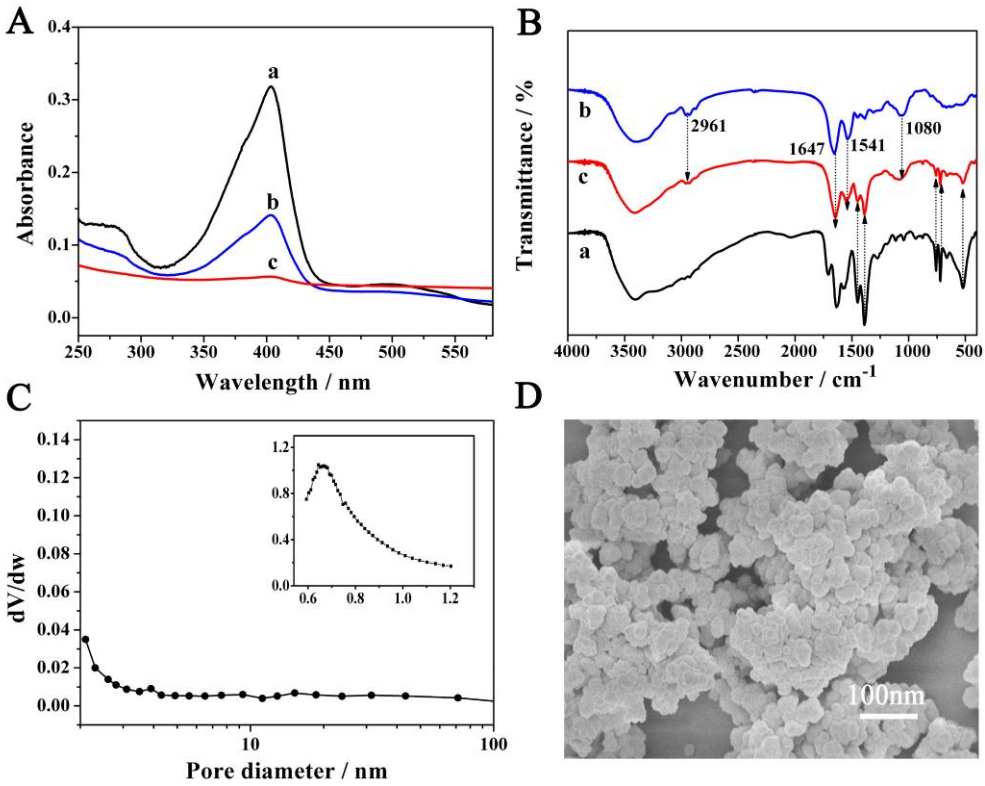

Fig. 2.

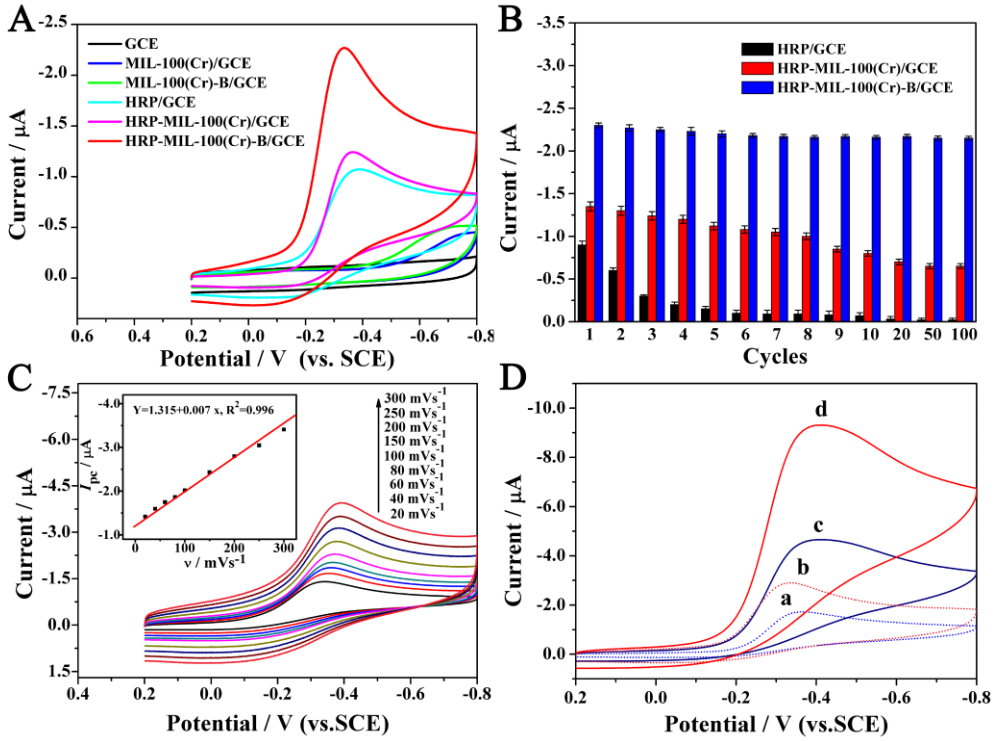

Fig. 3.

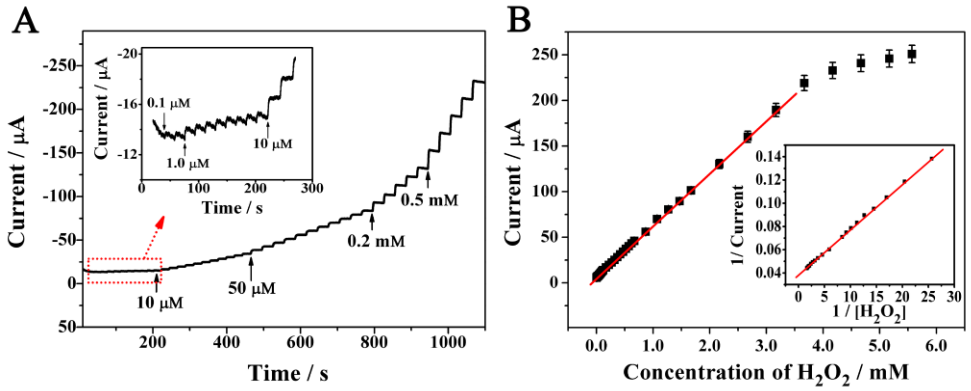

Fig. 4.

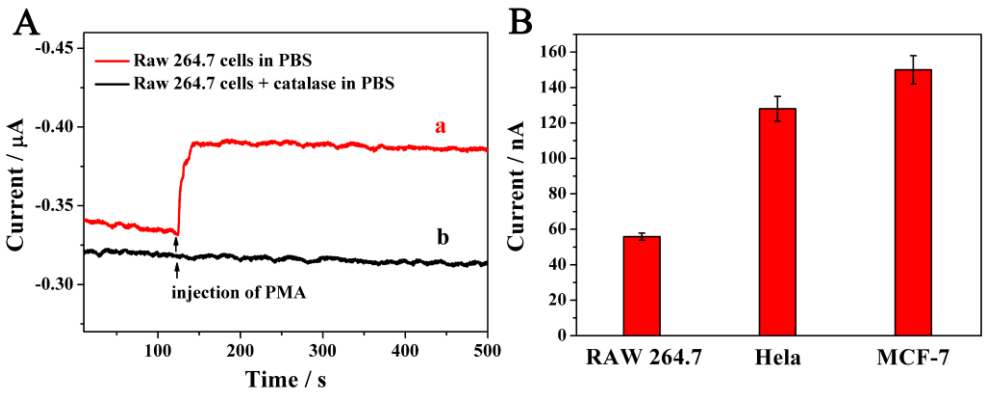

Highlights

- Hierarchically porous MIL-100(Cr)-B was used for the immobilization of HRP.
- The biosensor is durable for high sensitive and selective detection of H_2O_2.
- The biosensor has been successfully used to the real-time detection of H_2O_2 released from living cells.